New genetic tools for mushroom body output neurons in Drosophila

Gerald M. Rubin and Yoshinori Aso
Janelia Research Campus, Howard Hughes Medical Institute, Ashburn, United States

Abstract

How memories of past events influence behavior is a key question in neuroscience. The major associative learning center in Drosophila, the Mushroom Body (MB), communicates to the rest of the brain through Mushroom Body Output Neurons (MBONs). While 21 MBON cell types have their dendrites confined to small compartments of the MB lobes, analysis of EM connectomes revealed the presence of an additional 14 MBON cell types that are atypical in having dendritic input both within the MB lobes and in adjacent brain regions. Genetic reagents for manipulating atypical MBONs and experimental data on their functions has been lacking. In this report we describe new cell-type-specific GAL4 drivers for many MBONs, including the majority of atypical MBONs. Using these genetic reagents, we conducted optogenetic activation screening to examine their ability to drive behaviors and learning. These reagents provide important new tools for the study of complex behaviors in Drosophila.

Introduction

The Mushroom Body (MB) is the major site of associative learning in insects (reviewed in (Heisenberg, 2003; Modi et al., 2020). In the MB of each Drosophila brain hemisphere, multiple modalities of sensory stimuli are represented by the sparse activity of ~2000 Kenyon cells (KCs) whose parallel axonal fibers form the MB lobes. The lobes are further divided into compartments by the innervation patterns of dopaminergic neuron (DAN) axons and mushroom body output neuron (MBON) dendrites. MBONs provide the convergence element of the MB's three layer divergent-convergent circuit architecture and the outputs of the MBONs drive learned behaviors.

Whereas the dendrites of typical MBONs are strictly confined to the MB lobes, analysis of the Drosophila connectome in larvae (Eichler et al., 2017) and adults (Li et al., 2020; Scheffer et al., 2020) revealed a new class of "atypical" MBONs, consisting of 14 cell types in adults, that have part of their dendritic arbors outside the MB lobes, allowing them to integrate input from KCs with other information (Li et al., 2020). Some atypical MBONs receive dendritic input from other MBONs. Several provide output onto dopaminergic neurons (DANs) that innervate the MB to participate in recurrent networks. At least five make strong, direct synaptic contact onto descending neurons that drive motor action. Three provide strong direct connections to tangential neurons of the fan-shaped body of the central complex. However, analysis of the behaviors mediated by atypical MBONs has been limited by the lack of genetic drivers needed to manipulate their activity.

Here we report the generation and characterization of cell-type-specific split-GAL4 driver lines for the majority of the atypical MBONs. We also provide driver lines for two typical MBON types for which cell-type-specific split-GAL4 drivers were not previously available, and improved drivers for several other MBONs. We demonstrate the use of these new split-GAL4 lines in two behavioral assays. Using a four-armed olfactory arena equipped with optogenetic LED panels (Aso and Rubin, 2016; Pettersson, 1970), we assessed the ability of the labeled neurons to act as the unconditioned stimulus in an olfactory learning assay, an indication of their regulation of the activity of DANs. We also measured the effects of their optogenetic activation on kinematic parameters relevant for olfactory navigation. These reagents provide important new tools for the study of complex behaviors in Drosophila.

Results and Discussion

Generation and characterization of split-GAL4 lines for MBONs

We generated split-GAL4 genetic driver lines corresponding to MBON cell type using well-established methods (Dionne et al., 2018; Luan et al., 2006; Pfeiffer et al., 2010; Tirian and Dickson, 2017). The morphologies of the MBONs, produced by electron microscopic reconstruction, were used to search databases of light microscopic images to identify enhancers whose expression patterns might yield clean driver lines for that MBON when intersected (Mais et al., 2021; Meissner et al., 2023). We took advantage of an expanded set of starting reagents that were not available when Aso et al. (2014a) generated the original set of split-GAL4 drivers for the MB cell types; in addition to the ~7,000 GAL4 expression patterns described in (Jenett et al., 2012), we had access to an additional ~9,000 GAL4 expression patterns (Tirian and Dickson, 2017). A total of approximately 600 intersections were experimentally tested to generate the split-GAL4 lines reported here.

Figure 1 shows examples of expression patterns of some of the highest quality split-GAL4 lines. For many cell types we were able to identify multiple different split-GAL4 lines. The brain and ventral nerve cord expression patterns of all split-GAL4 lines are shown in Figure 1—figure supplement 1 for atypical MBONs and Figure 1—figure supplement 2 for typical MBONs. The original confocal stacks from which these Figures were generated, as well as additional image data, are available for download at https://splitgal4.janelia.org. Videos 1 and 2 provide examples of comparisons between light microscopic images from these lines and neuronal skeletons from the hemibrain dataset (Scheffer et al., 2020) that were used to confirm the assignment of cell type identity. Figure 1—figure supplement 3 summarizes what we consider to be the best available split-GAL4 lines for each of the MBON types identified by connectomics, based on a combination of the lines presented here and in previous studies. The expression patterns shown in this paper were obtained using an antibody against GFP which visualizes expression from 20xUAS-CsChrimson-mVenus in attP18. Directly visualizing the optogenetic effector is important since expression intensity, the number of labeled MBONs and off-targeted expression can differ when other UAS-reporter/effectors are used (for an example, see Figure 2—figure supplement 1 of Aso et al., 2014a).

For typical MBONs, we provide split-GAL4 lines for two cell types for which drivers were not described in (Aso et al., 2014a), MBON21 and MBON23. We also provide improved lines for MBON04 and MBON19; previous drivers for MBON04 also had expression in other MBON cell types and our new line for MBON19 has less off-target expression (see Aso et al., 2014a for previous lines).

For atypical MBONs we were able to generate multiple, independent driver lines for MBON20, MBON29, MBON30 and MBON33 that provide strong and specific expression. Several lines for MBON31 were generated, but they are also stochastically expressed in MBON32. Lines for MBON26 and MBON35 have some off-target expression that might compromise their use in behavioral assays, but they should permit cell-type-specific imaging studies. We failed to generate lines for MBON24, MBON25, MBON27, MBON32 and MBON34. We identified two candidate lines for MBON28 but because the morphology of MBON28 is very similar to those of MBON16 and MBON17 we were not able to make a definative cell type assignment (see Figure 1—figure supplement 3).

Activation phenotypes of MBON lines

MBONs are the first layer of neurons that transform memories stored inside the MB into actions. MBONs can also provide input to the dendrites of the DANs that innervate the MB lobes, forming a recurrent network. To investigate these two aspects of MBON function, we used a four-armed olfactory arena equipped with LED panels for optogenetics (Figure 2A). A group of ~20 starved flies that express CsChrimson in a particular MBON cell type was subjected to a series of optogenetic olfactory conditioning and memory tests, and then to six trials of activation in the absence of odors but with airflow (Figure 2B). Using the same setup and similar protocols, we have previously characterized the dynamics of memories formed by optogenetically activating DAN cell types innervating different MB compartments (Aso and Rubin, 2016) and analyzed circuits downstream of the MBONs that promote upwind locomotion (Aso et al., 2023). Figure 2C displays the results of these behavioral experiments sorted by the mean memory score of each cell type in the final memory test. When possible, we ran multiple independent split-GAL4 lines for the same MBON cell type. The concurrence of phenotypes in these cases provides further evidence that the observed effects are due to the activation of that cell type rather than off-target expression or genetic background effects.

Training flies by paring odor presentation with activation of MBON21, using either of the two lines tested (SS81853 and SS81521), resulted in robust aversive memory (Figure 2C) as previously observed with another driver for this cell type that displayed weaker expression (see SS46348 in Figure 1-figure supplement 2)(Otto et al., 2020). Both driver lines for the atypical MBON29 similarly induced aversive memory. These MBONs are both cholinergic, have dendrites in the γ4 and γ5 compartments, and synapse onto the dendrites of DANs that respond to punitive stimuli such as PAM-γ3 and PPL1-γ1pedc (Figure 2C, Figure 2-figure supplement 1) (Li et al., 2020; Otto et al., 2020). In contrast, training flies with activation of MBON33 induced appetitive memory. MBON33 is also cholinergic but preferentially connects with octopaminergic neurons and reward-representing DANs. We noticed that confocal microscopy images of MBON33 visualized by split-GAL4 contain additional branches around the esophagus (Figure 1H), an area which was outside of EM hemibrain volume. Since octopaminergic neurons arborize in this area, the connection between MBON33 and octopaminergic neurons might be more extensive than the previously described using the hemibrain data (Busch et al., 2009; Li et al., 2020).

To explore kinematic parameters controlled by MBONs, we tracked the trajectories of individual flies during and after a 10-second optogenetic stimulus (Figure 2C). Although we used the same flies that went through the optogenetic olfactory conditioning, the activation phenotypes of positive control lines could be observed and was not compromised by their prior activation (Figure 2-figure supplement 2). In these assays we observed some variability between lines for the same cell type, presumably due to difference in expression level or off-targeted expression. Nevertheless, the two lines for MBON21 showed similar patterns of kinematic variables: a low walking speed in the presence of the red activation light, a stimulus that caused elevated locomotion in genetic control flies, and then orientation toward upwind when the optogenetic stimulus concluded (Figures 2C and 3A-D). Similar phenotypes were observed with a driver for a combination of the three glutamatergic MBON01, MBON03 and MBON04 (MB011B; Figure 2C). Despite their common anatomical features and memory phenotypes, MBON21 and MBON29 modulated distinct motor parameters. Neither of the two lines for MBON29 changed walking speed or orientation toward upwind when activated, but they both increased angular motion at the onset of activation, similar to the three lines for MBON26 (Figure 3E-G).

Finally, we asked if the MBON21, MBON29 and MBON33 lines that were able to serve as the unconditioned stimulus in memory formation also drove corresponding avoidance or attraction. Previous studies and the results shown in Figures 2C indicated that these are not always shared phenotypes; for example, the set of glutamatergic MBONs in MB011B whose dendrites lie in the γ5 and β′2 compartments, can drive downwind locomotion and avoidance behaviors (Aso et al., 2023, 2014b; Matheson et al., 2022) but do not induce aversive memory. We tested if flies expressing CsChrimson in each of these three MBON cell types prefer quadrants of the arena with red activating light during the first and second 30s test periods (Figure 3H,I). When CsChrimson is expressed in MBON21 or MBON29, flies avoid illuminated quadrants of the arena. Conversely, CsChrismon activation in a line for MBON33 promoted attraction to the illuminated quadrants, although this effect was observed only at the first test period. Thus, in the case of these three MBON cell types, memory formation and avoidance/attraction behaviors are correlated.

Concluding Remarks

We generated and anatomically characterized an improved set of genetic driver lines for MBONs and provide the first driver lines for atypical MBONs. We expect these lines to be useful in a wide range of studies of fly behavior. We demonstrate the suitability of these lines for behavioral analyses by showing that multiple independent lines for the same cell type gave consistent results when assayed for their ability to serve as the unconditioned stimulus in memory formation and to produce appetitive or aversive movements. MBON21, MBON29 and MBON33, characterized in this study, have distinct features compared to well-studied MBONs that innervate the same compartments. MBON21 and MBON29 form cholinergic connections to the dendrites of DANs known to respond to punishment, whereas other MBONs from the same compartments form glutamatergic connections with reward-representing DANs (Figure 4A).

While most of sensory input to the MB is olfactory, the connectome revealed that two specific classes of Kenyon cells receive predominantly visual input. MBON19 provides the major output from one of these classes, KC α/βp, and about half of MBON19's sensory input is estimated to be visual. MBON33 provides a major output from the other class of visual KCs, KC γd, with more than half of the sensory input to its dendrites in the MB estimated to be visual. The cell-type-specific driver lines we provide for MBON19 and MBON33 should facilitate studies of the behavioral roles of the two streams of visual information that pass through the MB.

The MB and the central complex (CX) are thought to play key roles in the most cognitive processes that the fly can perform including learning, memory, and spatial navigation. Two of the MBONs for which we generated cell-type-specific driver lines, MBON21 and MBON30, provide the strongest direct inputs to the CX from the MB (Figure 4B), while MBON30 receives over three percent of its input (450 synapses) from the CX cell type FR1 (aka FB2-5RUB). The genetic reagents we report here should advance studies of reinforcement signals in parallel memory systems, the role of visual inputs to the MB, and information flow from the MB to the CX.

Materials and Methods

Flies

Split-GAL4 lines were created as previously described (Dionne et al., 2018). Flies were reared on standard cornmeal molasses food at 21-22℃ and 50% humidity. For optogenetic activation

experiments, flies were reared in the dark on standard food supplemented with retinal (Sigma-Aldrich, St. Louis, MO) unless otherwise specified, 0.2 mM all trans-retinal prior to eclosion and 0.4 mM all trans-retinal post eclosion. Female flies were sorted on cold plates and kept in retinal food vials for at least 1 day prior to be transferred to agar vials for 48-72 hours of starvation. Flies were 4-10 day old at the time of behavioral experiments. Images of the original confocal stacks for each of the lines are availabel at https://splitgal4.janelia.org.

The correspondence between the morphologies of EM skeletons and light microscopic images of GAL4 driver line expression patterns was used to assign GAL4 lines to particular cell types. This can be done with confidence when there are not multiple cell types with very similar morphology. However, in the case MBON28 we were not able to make a definitive assignment because of the similarity in the morphologies of MBON16, MBON17 and MBON28.

Immunohistochemistry and imaging

Dissection and immunohistochemistry of fly brains were carried out as previously described (Aso et al., 2014a). Each split-GAL4 line was crossed to the same Chrimson effector used for behavioral analysis. Full step-by-step protocols can be found at https://www.janelia.org/project-team/flylight/protocols. For single-cell labelling of neurons from selected split-Gal4 lines, we used the MultiColor FlpOut (MCFO) technique (Nern et al., 2015). Video 1 and Video 2 were produced using VVD Viewer (https://github.com/JaneliaSciComp/VVDViewer) to generate a video comparing light and EM data (hemibrain v1.2) for each cell type. Individual videos were then concatenated, and text added using Adobe Premiere Pro.

Optogenetics and olfactory learning assays

Groups of approximately 20 female flies were trained and tested at 25°C at 50% relative humidity in the fully automated olfactory arena for optogenetics experiments as previously described (Aso and Rubin, 2016; Pettersson, 1970; Vet et al., 1983). The 627nm peak LED light was used at 22.7 µW/mm2. The odors were diluted in paraffin oil (Sigma–Aldrich): Pentyl Acetate (PA; 1:10000) and Ethyl Lactate (EL; 1:10000). Videography was performed at 30 frames per second with 850nm LED backlight with 820nm longpass filter and analyzed using the Flytracker (Nath et al., 2013) and Fiji (Schindelin et al., 2012).

Statistics

Statistical comparisons were performed using the Kruskal Wallis test followed by Dunn's post-test for multiple comparison (Prism; Graphpad Inc, La Jolla, CA 92037). Appropriate sample size for olfactory learning experiment was estimated based on the standard deviation of performance index in previous study using the same assay (Aso and Rubin, 2016).

Connectomics

Information on connection strengths are taken from neuprint.janelia.org (hemibrain v1.2.1).

Data availability

The confocal images of expression patterns are available online (http://www.janelia.org/split-gal4). The source data for figures are included in the manuscript.

Acknowledgements

We thank the Janelia Fly Facility for help with fly husbandry and the FlyLight Project Team for dissection, histological preparation, and imaging of nervous systems. Marisa Dreher (Dreher Design Studios, Inc.) assembled the videos and helped with figure design. Claire Managan segmented the neuron morphologies shown in the videos. Masayoshi Ito helped identify lines to use in intersections. Daisuke Hattori, Glenn Turner, Vivek Jayaraman, Toshihide Hige and Yichun Shuai provided comments and suggestions on the early version of the manuscript.

References

Aso Y, Hattori D, Yu Y, Johnston RM, Iyer NA, Ngo T-TB, Dionne H, Abbott LF, Axel R, Tanimoto H, Rubin GM. 2014a. The neuronal architecture of the mushroom body provides a logic for associative learning. *Elife* **3**:e04577.

Aso Y, Herb A, Ogueta M, Siwanowicz I, Templier T, Friedrich AB, Ito K, Scholz H, Tanimoto H. 2012. Three dopamine pathways induce aversive odor memories with different stability. *PLoS Genet* **8**:e1002768.

Aso Y, Ray RP, Long X, Bushey D, Cichewicz K, Ngo T-T, Sharp B, Christoforou C, Hu A, Lemire AL, Tillberg P, Hirsh J, Litwin-Kumar A, Rubin GM. 2019. Nitric oxide acts as a cotransmitter in a subset of dopaminergic neurons to diversify memory dynamics. *Elife* **9**. doi:10.7554/eLife.64094

Aso Y, Rubin GM. 2016. Dopaminergic neurons write and update memories with cell-type-specific rules. *Elife* **5**. doi:10.7554/eLife.16135

Aso Y, Sitaraman D, Ichinose T, Kaun KR, Vogt K, Belliart-Guérin G, Plaçais P-Y, Robie AA, Yamagata N, Schnaitmann C, Rowell WJ, Johnston RM, Ngo T-TB, Chen N, Korff W, Nitabach MN, Heberlein U, Preat T, Branson KM, Tanimoto H, Rubin GM. 2014b. Mushroom body output neurons encode valence and guide memory-based action selection in Drosophila. *Elife* **3**:e04580.

Aso Y, Siwanowicz I, Bräcker L, Ito K, Kitamoto T, Tanimoto H. 2010. Specific dopaminergic neurons for the formation of labile aversive memory. *Curr Biol* **20**:1445–1451.

Aso Y, Yamada D, Bushey D, Hibbard KL, Sammons M, Otsuna H, Shuai Y, Hige T. 2023. Neural circuit mechanisms for transforming learned olfactory valences into wind-oriented movement. *Elife* **12**:e85756.

Bielopolski N, Amin H, Apostolopoulou AA, Rozenfeld E, Lerner H, Huetteroth W, Lin AC, Parnas M. 2019. Inhibitory muscarinic acetylcholine receptors enhance aversive olfactory learning in adult. *Elife* **8**. doi:10.7554/eLife.48264

Busch S, Selcho M, Ito K, Tanimoto H. 2009. A map of octopaminergic neurons in the Drosophila brain. *J Comp Neurol* **513**:643–667.

Chiang AS, Lin CY, Chuang CC, Chang HM, Hsieh CH, Yeh CW, Shih CT, Wu JJ, Wang GT, Chen YC, Wu CC, Chen GY, Ching YT, Lee PC, Lin CY, Lin HH, Wu CC, Hsu HW, Huang YA, Chen JY, Chiang HJ, Lu CF, Ni RF, Yeh CY, Hwang JK. 2011.Three-dimensional reconstruction of brain-wide wiring networks in Drosophila at single-cell resolution. Curr Biol. Jan 11:1-11. doi: 10.1016/j.cub.2010.11.056.

Claridge-Chang A, Roorda RD, Vrontou E, Sjulson L, Li H, Hirsh J, Miesenböck G. 2009. Writing memories with light-addressable reinforcement circuitry. *Cell* **139**:405–415.

Cohn R, Morantte I, Ruta V. 2015. Coordinated and Compartmentalized Neuromodulation Shapes Sensory Processing in Drosophila. *Cell* **163**:1742–1755.

Dionne H, Hibbard KL, Cavallaro A, Kao J-C, Rubin GM. 2018. Genetic Reagents for Making Split-GAL4 Lines in. *Genetics* **209**:31–35.

Eichler K, Li F, Litwin-Kumar A, Park Y, Andrade I, Schneider-Mizell CM, Saumweber T, Huser A, Eschbach C, Gerber B, Fetter RD, Truman JW, Priebe CE, Abbott LF, Thum AS, Zlatic M, Cardona A. 2017. The complete connectome of a learning and memory centre in an insect brain. *Nature* **548**:175–182.

Eckstein N, Bates AS, Du M, Hartenstein V, Jefferis GSXE, Funke, J. 2020. Neurotransmitter classification from electron microscopy images at synaptic sites in Drosophila. biorxiv.org/content/10.1101/2020.06.12.148775v2.full.

Eddison M, Ihrke G. 2022. Expansion-assisted iterative fluorescence in situ hybridization (EASI-FISH) in Drosophila CNS. dx.doi.org/10.17504/protocols.io.5jyl8jmw7g2w/v1.

Heisenberg M. 2003. Mushroom body memoir: from maps to models. *Nat Rev Neurosci* **4**:266–275.

Huetteroth W, Perisse E, Lin S, Klappenbach M, Burke C, Waddell S. 2015. Sweet taste and nutrient value subdivide rewarding dopaminergic neurons in Drosophila. *Curr Biol* **25**:751–758.

Hulse BK, Haberkern H, Franconville R, Turner-Evans D, Takemura S-Y, Wolff T, Noorman M, Dreher M, Dan C, Parekh R, Hermundstad AM, Rubin GM, Jayaraman V. 2021. A connectome of the Drosophila central complex reveals network motifs suitable for flexible navigation and context-dependent action selection. *Elife* **10**:e66039.

Ichinose T, Aso Y, Yamagata N, Abe A, Rubin GM, Tanimoto H. 2015. Reward signal in a recurrent circuit drives appetitive long-term memory formation. *Elife* **4**:e10719.

Jenett A, Rubin GM, Ngo T-TB, Shepherd D, Murphy C, Dionne H, Pfeiffer BD, Cavallaro A, Hall D, Jeter J, Iyer N, Fetter D, Hausenfluck JH, Peng H, Trautman ET, Svirskas RR, Myers EW, Iwinski ZR, Aso Y, DePasquale GM, Enos A, Hulamm P, Lam SCB, Li H-H, Laverty TR, Long F, Qu L, Murphy SD, Rokicki K, Safford T, Shaw K, Simpson JH, Sowell A, Tae S, Yu Y, Zugates CT. 2012. A GAL4-driver line resource for Drosophila neurobiology. *Cell Rep* **2**:991–1001.

Li F, Lindsey JW, Marin EC, Otto N, Dreher M, Dempsey G, Stark I, Bates AS, Pleijzier MW, Schlegel P, Nern A, Takemura S-Y, Eckstein N, Yang T, Francis A, Braun A, Parekh R, Costa M, Scheffer LK, Aso Y, Jefferis GS, Abbott LF, Litwin-Kumar A, Waddell S, Rubin GM. 2020. The connectome of the adult Drosophila mushroom body provides insights into function. *Elife* **9**. doi:10.7554/eLife.62576

Lin S, Owald D, Chandra V, Talbot C, Huetteroth W, Waddell S. 2014. Neural correlates of water reward in thirsty Drosophila. *Nat Neurosci* **17**:1536–1542.

Liu C, Plaçais P-Y, Yamagata N, Pfeiffer BD, Aso Y, Friedrich AB, Siwanowicz I, Rubin GM, Preat T, Tanimoto H. 2012. A subset of dopamine neurons signals reward for odour memory in Drosophila. *Nature* **488**:512–516.

Liu WW, Wilson RI. 2013. Glutamate is an inhibitory neurotransmitter in the Drosophila olfactory system. *Proc Natl Acad Sci U S A* **110**:10294–10299.

Luan H, Peabody NC, Vinson CR, White BH. 2006. Refined spatial manipulation of neuronal function by combinatorial restriction of transgene expression. *Neuron* **52**:425–436.

Mais L, Hirsch P, Managan C, Wang K, Rokicki K, Svirskas RR, Dickson BJ, Korff W, Rubin GM, Ihrke G, Meissner GW, Kainmueller D. 2021. PatchPerPixMatch for Automated 3d Search of Neuronal Morphologies in Light Microscopy. *bioRxiv*. doi:10.1101/2021.07.23.453511

Manoim JE, Davidson AM, Weiss S, Hige T, Parnas M. 2022. Lateral axonal modulation is required for stimulus-specific olfactory conditioning in Drosophila. *Curr Biol* **32**:4438–4450.e5.

Matheson AMM, Lanz AJ, Medina AM, Licata AM, Currier TA, Syed MH, Nagel KI. 2022. A neural circuit for wind-guided olfactory navigation. *Nat Commun* **13**:4613.

Meissner GW, Nern A, Dorman Z, DePasquale GM, Forster K, Gibney T, Hausenfluck JH, He Y, Iyer NA, Jeter J, Johnson L, Johnston RM, Lee K, Melton B, Yarbrough B, Zugates CT, Clements J, Goina C, Otsuna H, Rokicki K, Svirskas RR, Aso Y, Card GM, Dickson BJ, Ehrhardt E, Goldammer J, Ito M, Kainmueller D, Korff W, Mais L, Minegishi R, Namiki S, Rubin GM, Sterne GR, Wolff T, Malkesman O, FlyLight Project Team. 2023. A searchable image resource of Drosophila GAL4 driver expression patterns with single neuron resolution. *Elife* **12**. doi:10.7554/eLife.80660

Modi MN, Shuai Y, Turner GC. 2020. The Mushroom Body: From Architecture to Algorithm in a Learning Circuit. *Annu Rev Neurosci* **43**:465–484.

Nath T, Liu G, Weyn B, Hassan B, Ramaekers A, De Backer S, et al. Tracking for quantifying social network of Drosophila melanogaster. Lecture Notes in Computer Science (including subseries Lecture Notes in Artificial Intelligence and Lecture Notes in Bioinformatics). 2013. pp. 539–545. 10.1007/978-3-642-40246-3_67.

Otto N, Pleijzier MW, Morgan IC, Edmondson-Stait AJ, Heinz KJ, Stark I, Dempsey G, Ito M, Kapoor I, Hsu J, Schlegel PM, Bates AS, Feng L, Costa M, Ito K, Bock DD, Rubin GM, Jefferis GSXE, Waddell S. 2020. Input Connectivity Reveals Additional Heterogeneity of Dopaminergic Reinforcement in Drosophila. *Curr Biol* **30**:3200–3211.e8.

Pettersson J. 1970. An Aphid Sex Attractant. *Insect Syst Evol* **1**:63–73.

Pfeiffer BD, Ngo T-TB, Hibbard KL, Murphy C, Jenett A, Truman JW, Rubin GM. 2010. Refinement of tools for targeted gene expression in Drosophila. *Genetics* **186**:735–755.

Scheffer LK, Xu CS, Januszewski M, Lu Z, Takemura S-Y, Hayworth KJ, Huang GB, Shinomiya K, Maitlin-Shepard J, Berg S, Clements J, Hubbard PM, Katz WT, Umayam L, Zhao T, Ackerman D, Blakely T, Bogovic J, Dolafi T, Kainmueller D, Kawase T, Khairy KA, Leavitt L, Li PH, Lindsey L, Neubarth N, Olbris DJ, Otsuna H, Trautman ET, Ito M, Bates AS, Goldammer J, Wolff T, Svirskas R, Schlegel P, Neace E, Knecht CJ, Alvarado CX, Bailey DA, Ballinger S, Borycz JA, Canino BS, Cheatham N, Cook M, Dreher M, Duclos O, Eubanks B, Fairbanks K, Finley S, Forknall N, Francis A, Hopkins GP, Joyce EM, Kim S, Kirk NA, Kovalyak J, Lauchie SA, Lohff A, Maldonado C, Manley EA, McLin S, Mooney C, Ndama M, Ogundeyi O, Okeoma N, Ordish C, Padilla N, Patrick CM, Paterson T, Phillips EE, Phillips EM, Rampally N, Ribeiro C, Robertson MK, Rymer JT, Ryan SM, Sammons M, Scott AK, Scott AL, Shinomiya A, Smith C, Smith K, Smith NL, Sobeski MA, Suleiman A, Swift J, Takemura S, Talebi I, Tarnogorska D, Tenshaw E, Tokhi T, Walsh JJ, Yang T, Horne JA, Li F, Parekh R, Rivlin PK, Jayaraman V, Costa M, Jefferis GS, Ito K, Saalfeld S, George R, Meinertzhagen IA, Rubin GM, Hess HF, Jain V, Plaza SM. 2020. A connectome and analysis of the adult central brain. *Elife* **9**. doi:10.7554/eLife.57443

Schindelin J, Arganda-Carreras I, Frise E, Kaynig V, Longair M, Pietzsch T, Preibisch S, Rueden C, Saalfeld S, Schmid B, Tinevez JY, White DJ, Hartenstein V, Eliceiri K, Tomancak P, Cardona A. 2012. Fiji: an open-source platform for biological-image analysis. Nature Methods 9:676–682. doi: 10.1038/nmeth.2019.

Tirian L, Dickson BJ. 2017. The VT GAL4, LexA, and split-GAL4 driver line collections for targeted expression in the Drosophila nervous system. *bioRxiv*. doi:10.1101/198648

Vet LEM, van Lenteren JC, Heymans M, Meelis E. 1983. An airflow olfactometer for measuring olfactory responses of hymenopterous parasitoids and other small insects. Physiological Entomology 8:97–106. doi: https://doi.org/10.1111/j.1365-3032.1983.tb00338.x

Yamada D, Bushey D, Li F, Hibbard KL, Sammons M, Funke J, Litwin-Kumar A, Hige T, Aso Y. 2023. Hierarchical architecture of dopaminergic circuits enables second-order conditioning in Drosophila. *Elife* **12**. doi:10.7554/eLife.79042

Yamagata N, Hiroi M, Kondo S, Abe A, Tanimoto H. 2016. Suppression of Dopamine Neurons Mediates Reward. *PLoS Biol* **14**:e1002586.

Yamagata N, Ichinose T, Aso Y, Plaçais P-Y, Friedrich AB, Sima RJ, Preat T, Rubin GM, Tanimoto H. 2015. Distinct dopamine neurons mediate reward signals for short- and long-term memories. *Proc Natl Acad Sci U S A* **112**:578–583.

Zhao X, Lenek D, Dag U, Dickson BJ, Keleman K. 2018. Persistent activity in a recurrent circuit underlies courtship memory in Drosophila. *Elife* **7**:e31425.

Figure Legends

Figure 1: Selected images of new split-GAL4 lines. Panels A and C-H show expression (maximum intensity projections) of the indicated split-GAL4 line in the relevant portion of the brain. In panels A-H, the consensus JFRC2018 unisex brain template is also shown (green). Images showing the full brain, optic lobe and ventral nerve cord of these lines can be found in Figure 1—figure supplement 1 (for E-H) and Figure 1—figure supplement 2 (for A-D). Panels B, I and J show images derived from stochastic labeling that reveal the morphology of individual cells. The original confocal stacks from which these images were derived are available for download at https://splitgal4.janelia.org/cgi-bin/splitgal4.cgi.

Figure 1—figure supplement 1: Maximum intensity projections of the brains and ventral nerve cords of split-GAL4 lines for atypical MBON.

Figure 1—figure supplement 2: Maximum intensity projections of the brains and ventral nerve cords of split-GAL4 lines for typical MBON.

Figure 1—figure supplement 3: Summary list of selected split-GAL4 lines for all MBON cell types. These lines represent what we believe to be the best available split-GAL4 drivers for each cell type. The MB compartments they innervate and neurotransmitters are shown. The neurotransmitters that are shaded in gray were assigned based solely on computational prediction (Eckstein et al., 2020). Other transmitters have been confirmed by antibody staining (Aso et al., 2014) or EASI-FISH (Eddison and Ihrke 2022). The number of cells per hemisphere are shown for each cell type. Available split-GAL4 are listed. Lines listed in boldface are generally of higher quality. Lines whose names are shown in purple font were generated as part of this study. Lines whose names are shown in black font were described in Aso et al., 2014. Lines from other studies are shown brown font and their sources were as follows: SS01308, Aso et al., 2019; G0239, Chiang et al, 2011; SS46348, Otto et al., 2020; MB618B, SS01127, SS01188, SS01194, SS01298, SS01337 and SS01388, Aso 2021 release: https://splitgal4.janelia.org.

Figure 2. Behavioral consequences of optogenetic activation. (A) The four-armed olfactory arena. Approximately 20 starved female flies were confined in 10 cm diameter and 3 mm high circular area with a hole at the center for air suction. Odor was introduced through four channels at the corners. (B) The protocol for behavioral experiments. Flies were trained by pairing 60s of odor A with 30 1-second pulses of 627 nm LED light, each separated by 1s without illumination. A different odor, odor B, was presented without red LED illumination, and then preference between two odors was tested. In the reciprocal experiments, odor B was paired with red light and A was unpaired. The same training was repeated twice more and then a second odor preference test was performed. Finally, six cycles of 10-second 627nm illumination were applied, spaced by 100s intervals without odor. Airflow was maintained at 400 mL/min throughout the experiment. (C) Top: The memory scores at the second odor preference test, measured as preference indexes: [(number of flies in the paired odor quadrants)-(number of flies in the unpaired odor quadrants)]/total number of flies during the last 30s of the 60s test period. The red asterisks * and ** indicate $p<0.05$ or $p<0.01$, respectively: Dunn's multiple comparison tests compared to empty-split-GAL4 control, following Kruskal-Wallis test. The black * indicates $p<0.05$ without correction for multiple comparison. N=34 for the empty-split-GAL4 line and N=4-16 for other lines. All the lines were initially tested for 4 reciprocal experiments; lines with mean preference index above 0.1 or below -0.1 were subjected to additional tests. Cell types, the MB compartments in which their dendrites lie, their neurotransmitters, the number of synaptic connections they make with dopaminergic (DANs) and octopaminergic (OANs) neurons, and the split-GAL4 driver lines used for the behavioral assays are designated. A summary of connections from all MBON subtypes to DANs thought to signal reward or punishment and to OANs are shown in Figure 2—figure supplement 1A. Bottom: Z-scores [(values-mean)/standard deviation] for each parameter: Speed, walking speed; Angular, absolute of angular change relative to the previous frame at 30 FPS; cos(upwind), cosine of the fly's orientation toward the upwind direction (that is, facing away from the

center of the arena). ON periods correspond to the first 2s of the 10s LED ON periods, whereas OFF periods are the 2s immediately after the LEDs were turned off. Delta_DistanceFromCenter is change in fly's mean distance from the center of the arena relative to its position at the onset of LED illumination. Return is a measure of the probability that flies return to the position that they occupied at the end of the LED stimulus. Flies are judged to have returned if they move 10 mm or more from their original position and then return to within 3 mm of the original position within 15s.

Figure 2—figure supplement 1. Direct connections from MBONs to DANs and OANs.
(A) Total number of synaptic connections from each MBON type to DANs and OANs. Based on the valence of memory when activation of DANs is used as unconditioned stimulus in olfactory conditioning (Aso et al., 2012, 2010; Aso and Rubin, 2016; Claridge-Chang et al., 2009; Huetteroth et al., 2015; Ichinose et al., 2015; Lin et al., 2014; Liu et al., 2012; Yamada et al., 2023; Yamagata et al., 2016, 2015) we considered PAM01, 02, 04, 05, 06, 07, 08, 09, 10, 11 and 15 as Reward DANs and PAM12, 13, 14, PPL101, 103 and 106 as Punishment DANs. OANs refer to the four types of octopaminergic neurons that innervate the MB: OA-VPM3, OA-VPM4, OA-VUMa2 and OA-VUMa7. (B) Number of connections from MBONs in γ4 and γ5 to DANs in the γ lobe. PPL103, a DAN in the γ2 compartment, has less than five connections with these MBONs and was not included in this table.

Figure 2—figure supplement 2. Activation phenotypes are not compromised by prior optogenetic olfactory conditioning.
Time course of five kinematic parameters shown in Figure 2 for the positive control lines (MB011B and SS49755), negative control (Empty-split-GAL4), and two lines for MBON33 (SS75200 and SS77383) are shown. Lines and dashed lines represent mean of 6 trial averages for experiments with or without prior optogenetic conditioning sessions shown in Figure 2B. Lines and shadings are means and SEMs.

Figure 3. Additional behavioral consequences of optogentic activation.
(A) Time course of mean cos(upwind angle) for flies that express CsChrimson in MBON21 with designated drivers. The trace of empty-split-GAL4 is also shown. All the trajectories from six trials of movies were pooled to calculate a mean for each group of flies. Lines and shadings are means and SEMs.
(B) Mean cos(upwind angle) during 2 seconds periods immediately after LED was turned off.
(C-D) Time course and mean walking speed during 10s LED On period.
(E-F) The mean cumulative turning angles in 5 movie frames of (total elapsed time150 ms) for flies expressing CsChrimson in MBON29 and MBON26.
(G) The cumulative turning angle during the first 2 seconds of LED On period. (A-G) show data from the experiments described in Figure 2.
(H) Preference for quadrants with red light. Flies expressing CsChrimson in MBON21, MBON29 or MBON33 were tested with 30s continuous light of 627nm LED in two quadrants. The test was performed a second time with illumination in opposite quandrants after an 150s recovery period.
(I) Mean preference index to the quadrants with red light during the last 5s of two 30s test periods. Dunn's multiple comparison tests compared to empty-split-GAL4 control, following Kruskal-Wallis test. *, ** and *** indicate $p<0.05$, $p<0.01$ or $p<0.001$, respectively: N=66 for Empty-split-GAL4 and 8-22 for other lines in (A-G). N=16-26 in (H-I).

Figure 4 Diagrammatic summary of key outputs from selected MBONs. (A) MBON21 and MBON29 arborize dendrites in the g4 and g5 compartments that are innervated by reward representing DANs. MBON21 and MBON29 are cholinergic and preferentially connect with DANs that innervate other compartments to represent punishment, whereas other glutamatergic MBONs from these same compartments preferentially form connections with reward representing DANs going back to the same compartments. In fly brains, acetylcholine (ACh) is largely excitatory via nicotinic ACh receptors,

although the type A muscarinic ACh receptor can mediate an inhibitory effect (Bielopolski et al., 2019; Manoim et al., 2022). Glutamate (Glu) can be inhibitory or excitatory depending on the receptors in the postsynaptic cells. Glutamate is known to be inhibitory via the glutamate-gated chloride channel (GluClα) in the olfactory system (Liu and Wilson, 2013). All of the ten types of DANs examined with RNA-seq express GluClα and Nmdar2 at high levels whereas expression of Nmdar1 and other glutamate receptors were limited and cell type specific (Aso et al., 2019). Results in some studies support an excitatory effect of at least a subset of glutamatergic MBONs on DANs (Cohn et al., 2015; Ichinose et al., 2015; Otto et al., 2020; Zhao et al., 2018), while electrophysiological recordings identified inhibitory connection between glutamatergic MBON and the downstream interneurons (Aso et al., 2023). (B) Diagram showing direct connections between the MB and CX mediated by MBON21, MBON30, MBON09 and MBON04; these MBONs rank first, second, fifth and seventh, respectively, based on the number of direct synaptic connections to the CX; numbers reflect connections between right hemisphere MBONs and right hemisphere FB tangential cells. For circles representing MBONs, the circle diameter represents the fraction of that MBONs direct output that goes to the CX. For the downstream neurons in the CX, circle diameter represents the fraction of that cell types direct input that comes from MBONs. Arrow width reflects synapse number. See Figure 19 of (Li et al., 2020) and Figure 46 of (Hulse et al., 2021) for additional information on the complete set of MB to CX connections.

Video 1: Comparison of light microscopic images of atypical MBONs with hemibrain skeletons of the corresponding cell types.

Video 2: Comparison of light microscopic images of typical MBONs with hemibrain skeletons of the corresponding cell types

Appendix 1—key resources table

Reagent type (species) or resource	Designation	Source or reference	Identifiers	Additional information
strain, strain background (*Drosophila melanogaster*)	split-GAL4 lines	This paper (Aso et al. 2014) ; PMID: 25535793	https://splitgal4.janelia.org/cgi-bin/splitgal4.cgi	Available from Aso lab and Rubin lab
strain, strain background (*Drosophila melanogaster*)	20xUAS-CsChrimson-mVenus attP18	(Klapoetke et al. 2014); PMID: 24509633	N.A.	
strain, strain background (*Drosophila melanogaster*)	pJFRC200-10xUAS-IVS-myr::smGFP-HA in attP18	(Nern et al. 2015); PMID: 25964354	N.A.	

strain, strain background (*Drosophila melanogaster*)	pJFRC225-5xUAS-IVS-myr::smGFP-FLAG in VK00005	(Nern et al. 2015); PMID: 25964354	N.A.	
strain, strain background (*Drosophila melanogaster*)	pBPhsFlp2::PEST in attP3	(Nern et al. 2015); PMID: 25964354	N.A.	
strain, strain background (*Drosophila melanogaster*)	pJFRC201-10XUAS-FRT>STOP > FRT-myr::smGFP-HA in VK0005	(Nern et al. 2015); PMID: 25964354	N.A.	
strain, strain background (*Drosophila melanogaster*)	pJFRC240-10XUAS-FRT>STOP > FRT-myr::smGFP-V5-THS-10XUAS-FRT>STOP > FRT-myr::smGFP-FLAG_in_su(Hw)attP1	(Nern et al. 2015); PMID: 25964354	N.A.	
strain, strain background (*Drosophila melanogaster*)	empty-split-GAL4 (p65ADZp attP40, ZpGAL4DBD attP2)	(Hampel et al. 2015); PMID: 26344548	RRID:BDSC_79603	
antibody	anti-GFP (rabbit polyclonal)	Invitrogen	A11122 RRID:AB_221569	1:1000
antibody	anti-Brp (mouse monoclonal)	Developmental Studies Hybridoma Bank	nc82 RRID:AB_2341866	1:30
antibody	anti-HA-Tag (mouse monoclonal)	Cell Signaling Technology	C29F4; #3724 RRID:AB_10693385	1:300
antibody	anti-FLAG (rat monoclonal)	Novus Biologicals	NBP1-06712 RRID:AB_1625981	1:200
antibody	anti-V5-TAG Dylight-549 (mouse monoclonal)	Bio-Rad	MCA2894D549GA RRID:AB_10845946	1:500
antibody	anti-mouse IgG(H&L) AlexaFluor-568 (goat polyclonal)	Invitrogen	A11031 RRID:AB_144696	1:400

antibody	anti-rabbit IgG(H&L) AlexaFluor-488 (goat polyclonal)	Invitrogen	A11034 RRID:AB_2576217	1:800
antibody	anti-mouse IgG(H&L) AlexaFluor-488 conjugated (donkey polyclonal)	Jackson Immuno Research Labs	715-545-151 RRID:AB_2341099	1:400
antibody	anti-rabbit IgG(H&L) AlexaFluor-594 (donkey polyclonal)	Jackson Immuno Research Labs	711-585-152 RRID:AB_2340621	1:500
antibody	anti-rat IgG(H&L) AlexaFluor-647 (donkey polyclonal)	Jackson Immuno Research Labs	712-605-153 RRID:AB_2340694	1:300
antibody	anti-rabbit IgG(H+L) Alexa Fluor 568 (goat polyclonal)	Invitrogen	A-11036 RRID:AB_10563566	1:1000
chemical compound, drug	Pentyl acetate	Sigma-Aldrich	109584	1:10000 in paraffin oil
chemical compound, drug	Ethyl lactate	Sigma-Aldrich	W244015	1:10000 in paraffin oil
chemical compound, drug	Paraffin oil	Sigma-Aldrich	18512	
software, algorithm	ImageJ and Fiji	NIH; (Schindelin et al. 2012)	https://imagej.nih.gov/ij/ http://fiji.sc/	
software, algorithm	MATLAB	MathWorks	https://www.mathworks.com/	
software, algorithm	Adobe Illustrator CC	Adobe Systems	https://www.adobe.com/products/illustrator.html	
software, algorithm	GraphPad Prism 9	GraphPad Software	https://www.graphpad.com/scientific-software/prism/	
software, algorithm	Caltech FlyTracker	(Eyjolfsdottir et al. 2014)	https://github.com/kristinbranson/FlyTracker	

software, algorithm	neuPrint	(Plaza et al. 2022)	https://neuprint.janelia.org/	
software, algorithm	Cytoscape	(Shannon et al. 2003)	https://cytoscape.org/	
software, algorithm	Janelia workstation	HHMI Janelia	https://doi.org/10.25378/janelia.8182256.v1	
software, algorithm	NeuTu	(Zhao et al., 2018)	https://github.com/janelia-flyem/NeuTu	
software, algorithm	VVD Viewer	(Wan et al., 2012)	https://github.com/takashi310/VVD_Viewer	
other	Grade 3 MM Chr Blotting Paper	Whatmann	3030–335	Used in glass vials with paraffin-oil diluted odours
other	mass flow controller	Alicat	MCW-200SCCM-D	Mass flow controller used for the olfactory arena

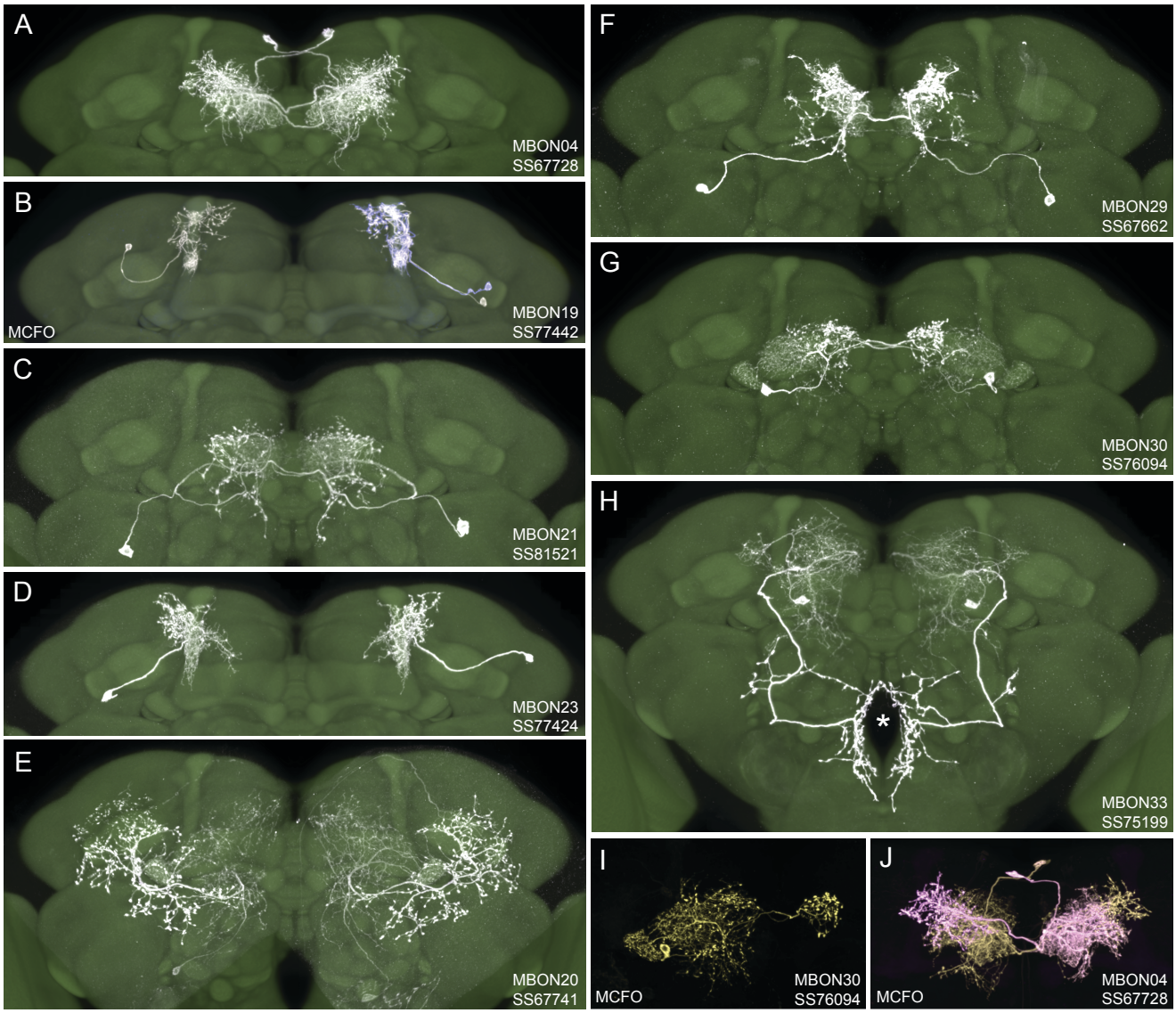
A
MBON04
SS67728
B
MCFO
MBON19
SS77442
C
MBON21
SS81521
D
MBON23
SS77424
E
MBON20
SS67741
F
MBON29
SS67662
G
MBON30
SS76094
H
*
MBON33
SS75199
I
MCFO
MBON30
SS76094
J
MCFO
MBON04
SS67728

Figure 1

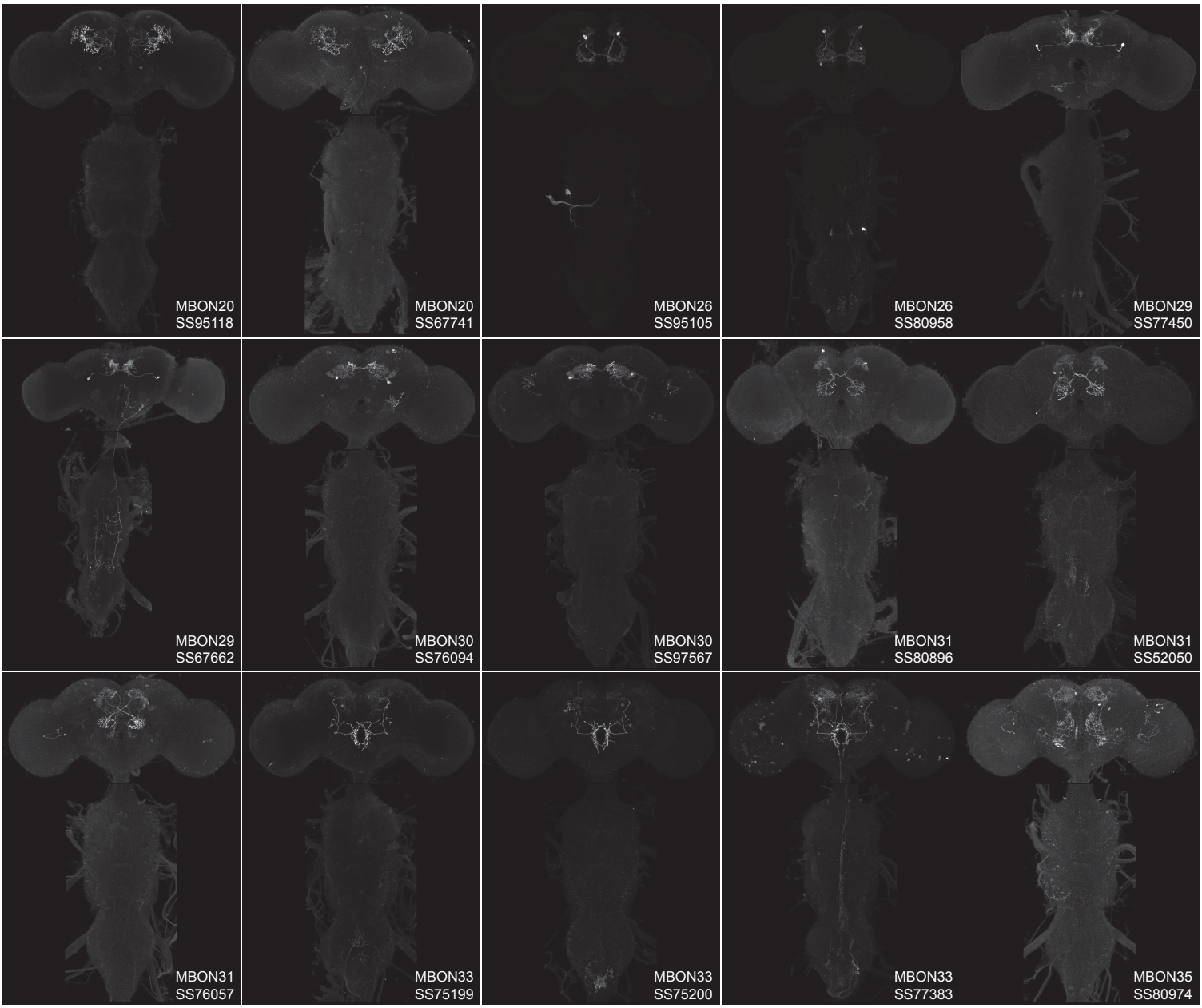

Figure 1-figure supplement 1

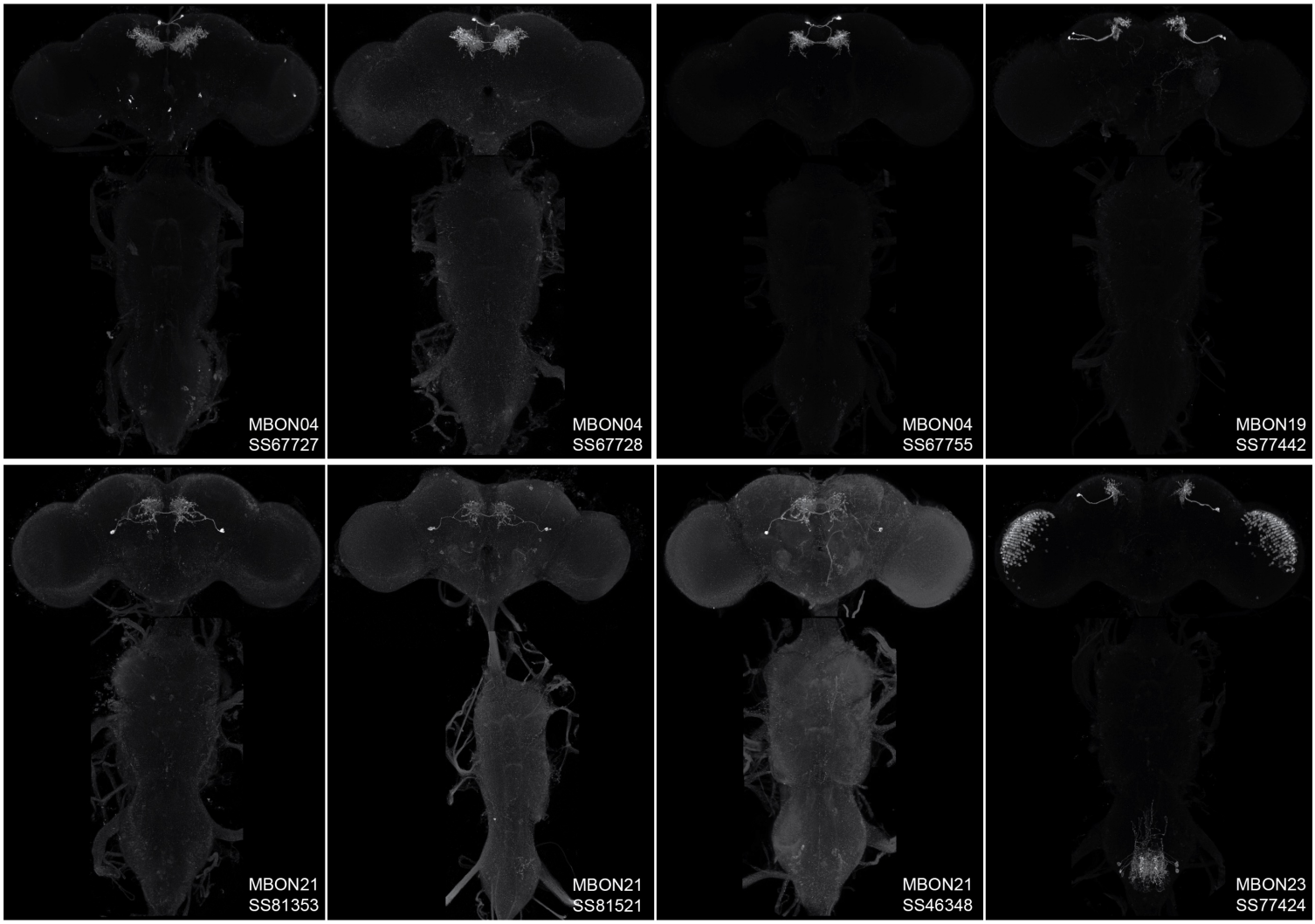

Figure 1-figure supplement 2

	Name	MB Compartments	Transmitter	Number of cells	Drivers
Typical MBONs	MBON01	γ5β′2a	Glutamate	1	**SS01308**, **MB011B**, **MB210B** (MB002B)
	MBON02	β2β′2a	Glutamate	1	MB399B, **SS01337**
	MBON03	β′2mp	Glutamate	1	**SS01127**, **MB002B**, **MB011B**, **MB210B**
	MBON04	β′2mp bilateral	Glutamate	1	**SS67727**, **SS67728**, **SS67755** (MB011B)
	MBON05	γ4>γ1γ2	Glutamate	1	**MB434B**, MB298B, SS01188
	MBON06	β1>α	Glutamate	1	**MB434B**, MB433B
	MBON07	α1	Glutamate	2	**MB310C**, **MB323B**, MB319C
	MBON08	γ3	GABA	0 or 1	**MB083C**, **MB110C**
	MBON09	γ3β′1	GABA	1 or 2	**MB083C**, **MB110C**
	MBON11	γ1pedc>α/β	GABA	1	**MB112C**, MB085C, MB262B
	MBON12	γ2α′1	Acetylcholine	2	**MB077B**, MB051B, MB090C
	MBON13	α′2	Acetylcholine	1	**MB018B**, MB091C
	MBON14	α3	Acetylcholine	2	MB082C, MB093C, G0239
	MBON15	α′1	Acetylcholine	4	MB543B, MB618B
	MBON16	α′3ap	Acetylcholine	1	**MB027B**, MB549C, **SS01298**
	MBON17	α′3m	Acetylcholine	2	**MB027B**, MB618B, **SS01298**
	MBON18	α2sc	Acetylcholine	1	**SS01194**, MB549C, MB080C, MB050B
	MBON19	α2p3p	Acetylcholine	2	**SS77442**, MB542B
	MBON21	γ4γ5	Acetylcholine	1	**SS81353**, **SS81521**,SS46348
	MBON22	calyx	Acetylcholine	1	**SS01388**, MB242A
	MBON23	α2sp	Acetylcholine	1	**SS77424**
Atypical MBONs	MBON10	β′1	GABA	3	MB057B, MB078C
	MBON20	γ1γ2	GABA	1	**SS67741**, **SS95118**
	MBON24	β2γ5	Acetylcholine	1	none
	MBON25	γ1γ2	Glutamate	1	none
	MBON26	β′2d	Acetylcholine	1	**SS80958**, **SS95105**, **SS95109**
	MBON27	γ5d	Acetylcholine	1	none
	MBON28	α′3a	Acetylcholine	1	candidates SS81557, SS86947
	MBON29	γ4γ5	Acetylcholine	1	**SS77450**, **SS67662**
	MBON30	γ1γ2γ3	Glutamate	1	**SS76094**, **SS97567**
	MBON31	α′1a	GABA	1	**SS52050**, SS76057, **SS80896**
	MBON32	γ2	GABA	1	none (SS76057 contains MBON31 & MBON32)
	MBON33	γ2γ3	Acetylcholine	1	**SS75199**, **SS75200**, SS77383
	MBON34	γ2	Glutamate	1	none
	MBON35	γ2	Acetylcholine	1	SS80974

Figure 1-figure supplement 3

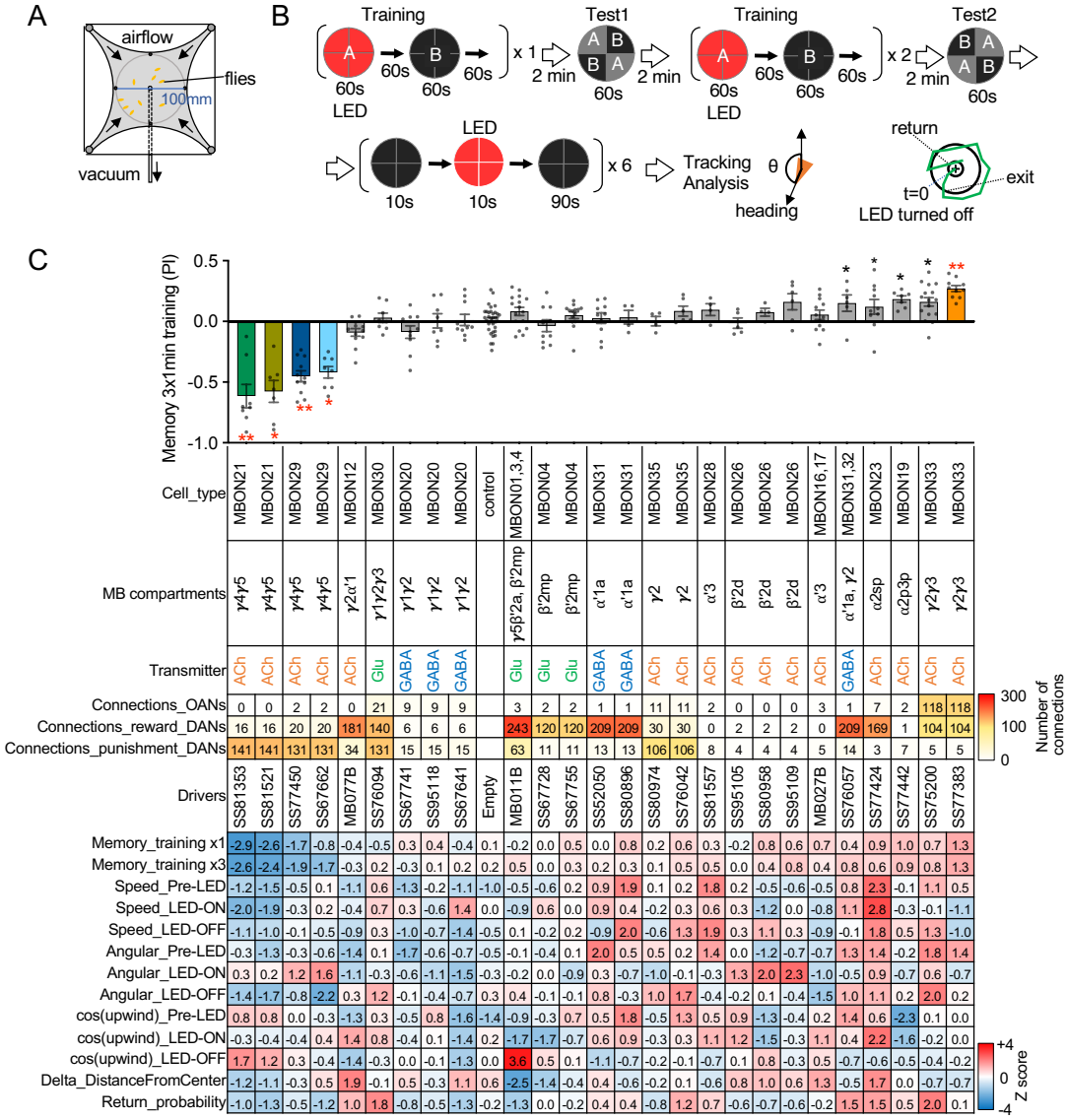
A
airflow
flies
100 mm
vacuum
B
Training
A
B
60s
60s
60s
LED
x 1
Test1
2 min
60s
2 min
Training
x 2
Test2
2 min
60s
LED
10s
10s
90s
x 6
Tracking Analysis
θ
heading
return
exit
t=0
LED turned off
C
Memory 3x1min training (PI)
0.5
0.0
-0.5
-1.0
Cell_type
MB compartments
Transmitter
Connections_OANs
Connections_reward_DANs
Connections_punishment_DANs
Drivers
Memory_training x1
Memory_training x3
Speed_Pre-LED
Speed_LED-ON
Speed_LED-OFF
Angular_Pre-LED
Angular_LED-ON
Angular_LED-OFF
cos(upwind)_Pre-LED
cos(upwind)_LED-ON
cos(upwind)_LED-OFF
Delta_DistanceFromCenter
Return_probability
300
100
0
Number of connections
+4
0
-4
Z score

Figure 2

A

From		To		
Cell type	transmitter	OANs	Reward DANs	Punishment DANs
MBON01	Glutamate	1	97	49
MBON02	Glutamate	10	116	0
MBON03	Glutamate	0	26	3
MBON04	Glutamate	2	120	11
MBON05	Glutamate	13	333	60
MBON06	Glutamate	4	188	19
MBON07	Glutamate	61	73	0
MBON09	GABA	1	147	48
MBON10	GABA	0	105	124
MBON11	GABA	97	91	96
MBON12	Acetylcholine	0	181	34
MBON13	Acetylcholine	1	78	9
MBON14	Acetylcholine	10	14	30
MBON15	Acetylcholine	2	40	384
MBON16	Acetylcholine	1	0	1
MBON17	Acetylcholine	2	0	4
MBON18	Acetylcholine	4	24	17
MBON19	Acetylcholine	2	1	7
MBON20	GABA	9	6	15
MBON21	Acetylcholine	0	16	141
MBON22	Acetylcholine	2	19	10
MBON23	Acetylcholine	7	169	3
MBON24	Acetylcholine	0	8	15
MBON25	Glutamate	0	35	22
MBON26	Acetylcholine	0	2	4
MBON27	Acetylcholine	1	0	3
MBON28	Acetylcholine	2	0	8
MBON29	Acetylcholine	2	20	131
MBON30	Glutamate	21	140	131
MBON31	GABA	1	209	13
MBON32	GABA	0	0	1
MBON33	Acetylcholine	118	104	5
MBON34	Glutamate	1	6	13
MBON35	Acetylcholine	11	30	106

B

			Punishment DANs		Reward DANs	
			γ1 PPL101	γ3 PAM12	γ4 PAM07, 08	γ5 PAM01
MBON21	γ4γ5	ACh	30	91	12	1
MBON29	γ4γ5	ACh	99	4	9	4
MBON05	γ4	Glu	11	13	285	15
MBON01	γ5β′2a	Glu	0	6	4	47

Figure 2-figure supplement 1

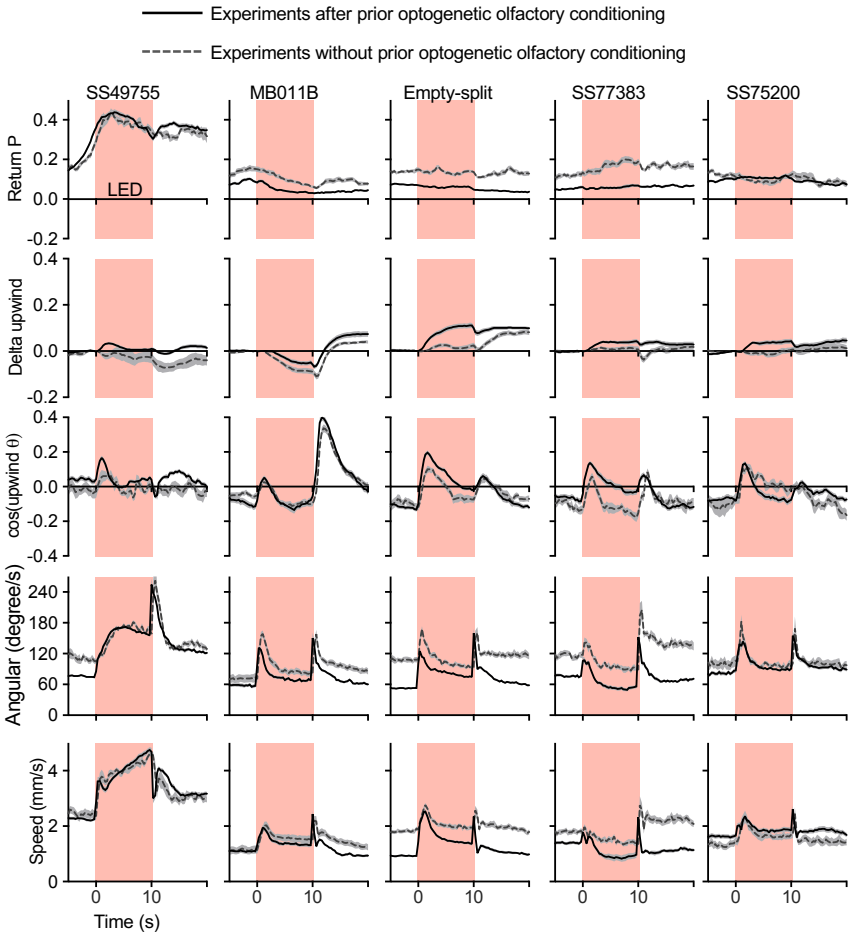

Figure 2-figure supplement 2

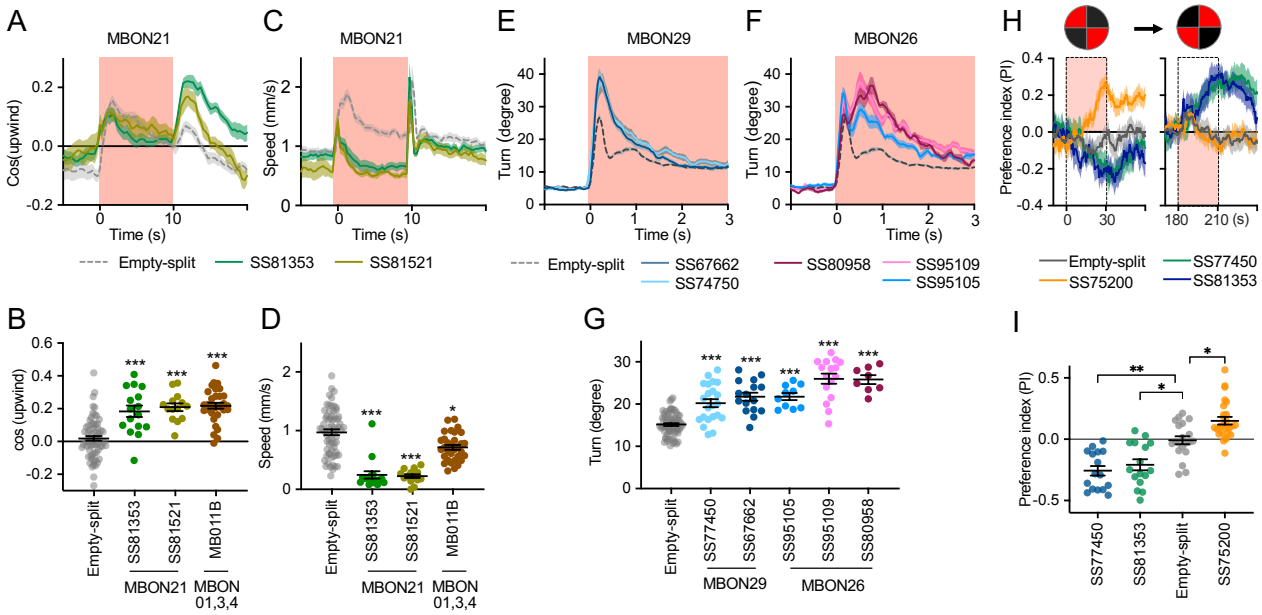
A
MBON21
Cos(upwind)
Time (s)
Empty-split
SS81353
SS81521
C
MBON21
Speed (mm/s)
Time (s)
E
MBON29
Turn (degree)
Time (s)
Empty-split
SS67662
SS74750
F
MBON26
Turn (degree)
Time (s)
SS80958
SS95109
SS95105
H
Preference index (PI)
Empty-split
SS75200
SS77450
SS81353
B
cos (upwind)
Empty-split
SS81353
SS81521
MB011B
MBON21
MBON 01,3,4
D
Speed (mm/s)
Empty-split
SS81353
SS81521
MB011B
MBON21
MBON 01,3,4
G
Turn (degree)
Empty-split
SS77450
SS67662
SS95105
SS95109
SS80958
MBON29
MBON26
I
Preference index (PI)
SS77450
SS81353
Empty-split
SS75200

Figure 3

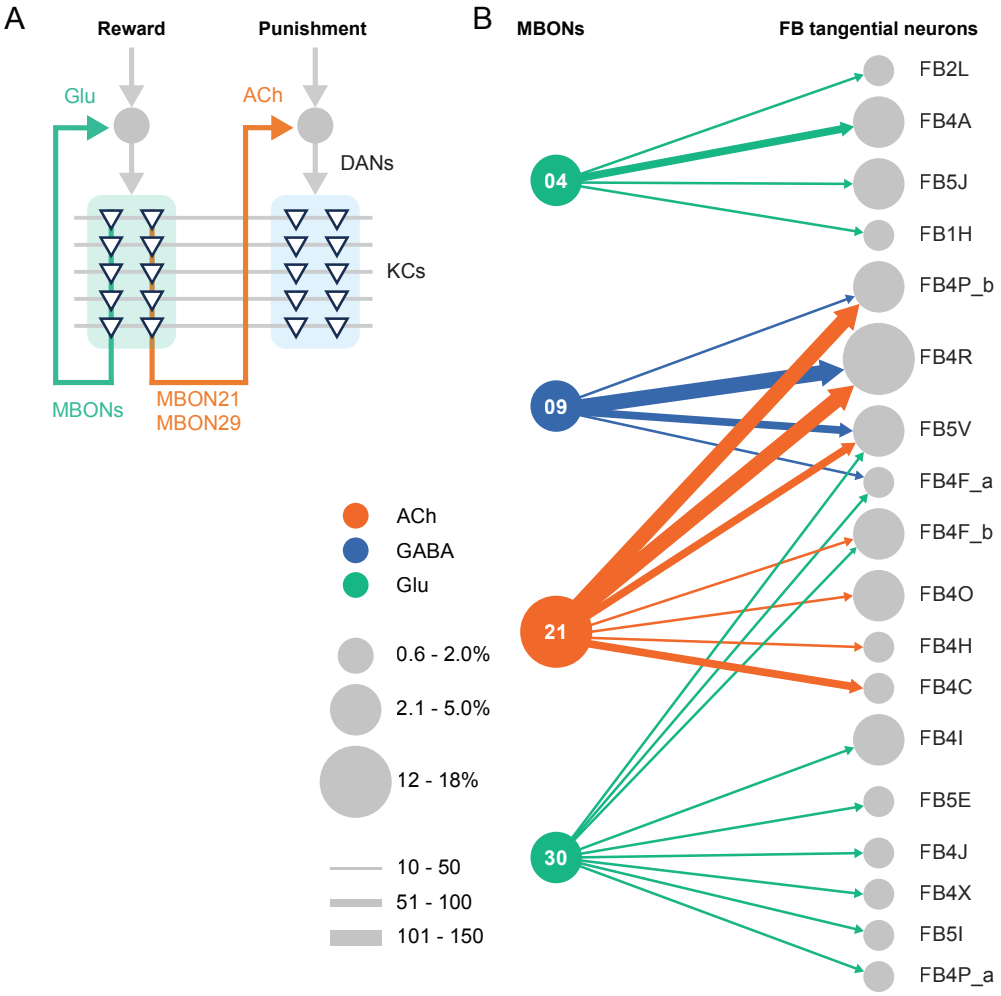
A
Reward
Punishment
Glu
ACh
DANs
KCs
MBONs
MBON21
MBON29
B
MBONs
FB tangential neurons
04
09
21
30
FB2L
FB4A
FB5J
FB1H
FB4P_b
FB4R
FB5V
FB4F_a
FB4F_b
FB4O
FB4H
FB4C
FB4I
FB5E
FB4J
FB4X
FB5I
FB4P_a
ACh
GABA
Glu
0.6 - 2.0%
2.1 - 5.0%
12 - 18%
10 - 50
51 - 100
101 - 150

Figure 4